

# A comparison of forward and backward $pp$ pair knockout in ${}^3\text{He}(e, e'pp)n$

H. Baghdasaryan,<sup>1,\*</sup> L.B. Weinstein,<sup>1,†</sup> J.M. Laget,<sup>32</sup> K.P. Adhikari,<sup>1</sup> M. Aghasyan,<sup>16</sup> M.J. Amarian,<sup>1</sup> M. Anghinolfi,<sup>17</sup> J. Ball,<sup>6</sup> M. Battaglieri,<sup>17</sup> A.S. Biselli,<sup>9,27</sup> W.J. Briscoe,<sup>13</sup> W.K. Brooks,<sup>33,32</sup> V.D. Burkert,<sup>32</sup> D.S. Carman,<sup>32</sup> A. Celentano,<sup>17</sup> S. Chandavar,<sup>26</sup> G. Charles,<sup>6</sup> P.L. Cole,<sup>14,32</sup> M. Contalbrigo,<sup>15</sup> V. Crede,<sup>11</sup> A. D'Angelo,<sup>18,29</sup> A. Daniel,<sup>26</sup> N. Dashyan,<sup>38</sup> E. De Sanctis,<sup>16</sup> R. De Vita,<sup>17</sup> C. Djalali,<sup>31</sup> G.E. Dodge,<sup>1</sup> D. Doughty,<sup>7,32</sup> R. Dupre,<sup>2,‡</sup> H. Egiyan,<sup>32,37</sup> A. El Alaoui,<sup>2</sup> L. El Fassi,<sup>2</sup> L. Elouadrhiri,<sup>32</sup> G. Fedotov,<sup>31</sup> M.Y. Gabrielyan,<sup>10</sup> N. Gevorgyan,<sup>38</sup> G.P. Gilfoyle,<sup>28</sup> K.L. Giovanetti,<sup>21</sup> F.X. Girod,<sup>32</sup> W. Gohn,<sup>8</sup> R.W. Gothe,<sup>31</sup> K.A. Griffioen,<sup>37</sup> B. Guegan,<sup>19</sup> M. Guidal,<sup>19</sup> K. Hafidi,<sup>2</sup> K. Hicks,<sup>26</sup> C.E. Hyde,<sup>1</sup> D.G. Ireland,<sup>34</sup> B.S. Ishkhanov,<sup>30</sup> D. Jenkins,<sup>35</sup> H.S. Jo,<sup>19</sup> K. Joo,<sup>8</sup> M. Khandaker,<sup>25</sup> P. Khetarpal,<sup>10</sup> A. Kim,<sup>22</sup> W. Kim,<sup>22</sup> A. Kubarovskiy,<sup>27,30</sup> V. Kubarovskiy,<sup>32,27</sup> S.E. Kuhn,<sup>1</sup> S.V. Kuleshov,<sup>33,20</sup> N.D. Kvaltine,<sup>36</sup> H.Y. Lu,<sup>4</sup> I.J.D. MacGregor,<sup>34</sup> B. McKinnon,<sup>34</sup> M. Mirazita,<sup>16</sup> V. Mokeev,<sup>32,30,§</sup> H. Moutarde,<sup>6</sup> E. Munevar,<sup>32</sup> S. Niccolai,<sup>19,13</sup> G. Niculescu,<sup>21,26</sup> I. Niculescu,<sup>21,32</sup> M. Osipenko,<sup>17</sup> M. Paolone,<sup>31</sup> L.L. Pappalardo,<sup>15</sup> R. Parenduyan,<sup>38</sup> K. Park,<sup>32,22</sup> S. Park,<sup>11</sup> S. Pisano,<sup>16</sup> S. Pozdniakov,<sup>20</sup> S. Procureur,<sup>6</sup> B.A. Raue,<sup>10,32</sup> G. Ricco,<sup>12,¶</sup> D. Rimal,<sup>10</sup> M. Ripani,<sup>17</sup> G. Rosner,<sup>34</sup> P. Rossi,<sup>16</sup> M.S. Saini,<sup>11</sup> N.A. Saylor,<sup>27</sup> D. Schott,<sup>10</sup> R.A. Schumacher,<sup>4</sup> H. Seraydaryan,<sup>1</sup> E.S. Smith,<sup>32</sup> D.I. Sober,<sup>5</sup> D. Soker,<sup>19</sup> S.S. Stepanyan,<sup>22</sup> S. Stepanyan,<sup>32</sup> S. Strauch,<sup>31,13</sup> M. Taiuti,<sup>12,¶</sup> W. Tang,<sup>26</sup> S. Tkachenko,<sup>36</sup> H. Voskanyan,<sup>38,\*\*</sup> E. Voutier,<sup>23</sup> M.H. Wood,<sup>3,31</sup> L. Zana,<sup>24</sup> and B. Zhao<sup>37</sup>

(The CLAS Collaboration)

<sup>1</sup>Old Dominion University, Norfolk, Virginia 23529

<sup>2</sup>Argonne National Laboratory, Argonne, Illinois 60439

<sup>3</sup>Canisius College, Buffalo, NY

<sup>4</sup>Carnegie Mellon University, Pittsburgh, Pennsylvania 15213

<sup>5</sup>Catholic University of America, Washington, D.C. 20064

<sup>6</sup>CEA, Centre de Saclay, Irfu/Service de Physique Nucléaire, 91191 Gif-sur-Yvette, France

<sup>7</sup>Christopher Newport University, Newport News, Virginia 23606

<sup>8</sup>University of Connecticut, Storrs, Connecticut 06269

<sup>9</sup>Fairfield University, Fairfield CT 06824

<sup>10</sup>Florida International University, Miami, Florida 33199

<sup>11</sup>Florida State University, Tallahassee, Florida 32306

<sup>12</sup>Università di Genova, 16146 Genova, Italy

<sup>13</sup>The George Washington University, Washington, DC 20052

<sup>14</sup>Idaho State University, Pocatello, Idaho 83209

<sup>15</sup>INFN, Sezione di Ferrara, 44100 Ferrara, Italy

<sup>16</sup>INFN, Laboratori Nazionali di Frascati, 00044 Frascati, Italy

<sup>17</sup>INFN, Sezione di Genova, 16146 Genova, Italy

<sup>18</sup>INFN, Sezione di Roma Tor Vergata, 00133 Rome, Italy

<sup>19</sup>Institut de Physique Nucléaire ORSAY, Orsay, France

<sup>20</sup>Institute of Theoretical and Experimental Physics, Moscow, 117259, Russia

<sup>21</sup>James Madison University, Harrisonburg, Virginia 22807

<sup>22</sup>Kyungpook National University, Daegu 702-701, Republic of Korea

<sup>23</sup>LPSC, Université Joseph Fourier, CNRS/IN2P3, INPG, Grenoble, France

<sup>24</sup>University of New Hampshire, Durham, New Hampshire 03824-3568

<sup>25</sup>Norfolk State University, Norfolk, Virginia 23504

<sup>26</sup>Ohio University, Athens, Ohio 45701

<sup>27</sup>Rensselaer Polytechnic Institute, Troy, New York 12180-3590

<sup>28</sup>University of Richmond, Richmond, Virginia 23173

<sup>29</sup>Università di Roma Tor Vergata, 00133 Rome Italy

<sup>30</sup>Skobeltsyn Nuclear Physics Institute, Skobeltsyn Nuclear Physics Institute, 119899 Moscow, Russia

<sup>31</sup>University of South Carolina, Columbia, South Carolina 29208

<sup>32</sup>Thomas Jefferson National Accelerator Facility, Newport News, Virginia 23606

<sup>33</sup>Universidad Técnica Federico Santa María, Casilla 110-V Valparaíso, Chile

<sup>34</sup>University of Glasgow, Glasgow G12 8QQ, United Kingdom

<sup>35</sup>Virginia Polytechnic Institute and State University, Blacksburg, Virginia 24061-0435

<sup>36</sup>University of Virginia, Charlottesville, Virginia 22901

<sup>37</sup>College of William and Mary, Williamsburg, Virginia 23187-8795

<sup>38</sup>Yerevan Physics Institute, 375036 Yerevan, Armenia

(Dated: November 11, 2018)

Measuring nucleon-nucleon Short Range Correlations (SRC) has been a goal of the nuclear physics community for many years. They are an important part of the nuclear wavefunction, accounting for

almost all of the high-momentum strength. They are closely related to the EMC effect. While their overall probability has been measured, measuring their momentum distributions is more difficult. In order to determine the best configuration for studying SRC momentum distributions, we measured the  ${}^3\text{He}(e, e'pp)n$  reaction, looking at events with high momentum protons ( $p_p > 0.35$  GeV/c) and a low momentum neutron ( $p_n < 0.2$  GeV/c). We examined two angular configurations: either both protons emitted forward or one proton emitted forward and one backward (with respect to the momentum transfer,  $\vec{q}$ ). The measured relative momentum distribution of the events with one forward and one backward proton was much closer to the calculated initial-state  $pp$  relative momentum distribution, indicating that this is the preferred configuration for measuring SRC.

PACS numbers: 21.45.-v 25.30.Dh

Early models of the nucleus described its structure in terms of individual nucleons moving independently of each other in a mean field. However, this only describes about 70% of the nucleus. The missing 30% is presumably due to nucleons in short and long range correlations [1].

Nucleon-nucleon ( $NN$ ) Short Range Correlations (SRC) are a very important part of the nuclear wave function. The two nucleons in an SRC are at comparatively short distances and thus higher densities than mean field nucleons. These SRC nucleons account for almost all of the high momentum ( $p > p_{fermi} \approx 0.25$  GeV/c) nucleons and most of the kinetic energy in the nucleus. Nucleons have a probability of between  $\approx 5\%$  (deuterium) and  $\approx 25\%$  ( $A \geq 56$ ) of belonging to an SRC pair [2–4].

SRC can affect the rate of neutron star cooling [5]. In the direct Urca process ( $p \rightarrow n + e^+ + \nu$  and  $n \rightarrow p + e^- + \bar{\nu}$ ), nucleons in the neutron star beta-decay and the neutrino carries energy away. However, the decay nucleon is frequently at a momentum below the Fermi-surface and then the process is Pauli-blocked. In the modified Urca process, a second nucleon is involved so that the decay products are no longer below the Fermi-surface and the process is not Pauli-blocked. SRC, by moving nucleons from below to above the Fermi-surface and opening holes in the Fermi-sphere, can also allow Urca-process cooling to occur.

In addition, it was recently found that the probability of a nucleon belonging to an SRC in nucleus  $A$  is remarkably closely correlated with the strength of the EMC effect as measured in lepton Deep Inelastic Scattering (DIS) in that nucleus [6]. The EMC effect is the decrease in the per-nucleon cross section of nucleus  $A$  relative to deuterium. This effect cannot be explained without including some modification of the nucleons in the nucleus [7]. The correlation indicates that SRC and the EMC effect stem from the same underlying cause and that nucleon modification in the nucleus is related to SRC.

The relative probabilities of finding nucleons belonging to SRC have been measured by inclusive ( $e, e'$ ) experiments. They measured the per-nucleon cross section ratio of nucleus  $A$  to deuterium [4, 8] or  ${}^3\text{He}$  [2, 3] at fixed four-momentum transfer  $Q^2$  ( $Q^2 = -q_\mu q^\mu = \vec{q}^2 - \nu^2$ ,

$\nu$  is the energy transfer, and  $\vec{q}$  is the three-momentum transfer) as a function of  $x = Q^2/2m\nu$  where  $m$  is the nucleon mass. There is a plateau in the cross section ratio for  $Q^2 > 1.5$  GeV<sup>2</sup> ranging from about  $1.5 < x < 2$ . Under certain reasonable assumptions (see references for details), the minimum initial struck-nucleon momentum is a function of only  $x$  and  $Q^2$ . The existence of this plateau indicates that nucleons have the same momentum distribution in different nuclei for momenta greater than some threshold. The location of the onset of the plateau in  $x$  and  $Q^2$  indicates that this threshold is  $p_{thresh} = 0.275 \pm 0.025$  GeV/c. The height of the plateau (the magnitude of the per-nucleon cross section ratio) corresponds to the relative probability of finding nucleons in the two nuclei for  $p > 0.275$  GeV/c.

Since the different nuclei ( $2 \leq A \leq 197$ ) have very different characteristics (density, radius, etc.), this similar momentum distribution at high momentum cannot be due to the  $A - 1$  other nucleons and thus can only be due to the presence of a single adjacent nucleon, *i.e.*, due to  $NN$  SRC. Thus the value of the per-nucleon cross section ratio in the plateau region equals the relative probability that nucleons in the two nuclei belong to short range correlations.

It is more difficult to measure the relative and total momentum distributions of the correlated nucleons. Measurements of the  ${}^3\text{He}(e, e'pp)n$  reaction studied events where the virtual photon is absorbed by the third nucleon and the other two nucleons belong to a spectator correlated pair which disintegrates in the absence of the third nucleon [9, 10]. The relative and total final state momenta,  $p_{rel}$  and  $p_{tot}$ , of the other two nucleons then should correspond to those quantities in the initial state. This measurement is complicated by the strong continuum-state interaction between those two nucleons in the final state. This technique also does not apply to nuclei heavier than  ${}^3\text{He}$ .

Efforts to measure the momentum distributions of correlated  $NN$  pairs in heavier nuclei focus on knocking out a high-initial-momentum nucleon (usually a proton) and detecting its correlated partner. This can be done with either proton [11, 12] or electron [13, 14] probes. However, the interpretation of these experiments can be complicated by the final state interaction of the knocked-out proton, as well as from the effects of two-body currents

such as meson exchange currents and isobar configurations (*e.g.*,  $\Delta(1232)$  production followed by de-excitation and absorption of the decay pion on another nucleon).

There are two general kinematic configurations for these measurements. The partner nucleon can be detected in the forward hemisphere relative to the momentum transfer  $\vec{q}$  or in the backward hemisphere. If the partner nucleon is detected in the forward hemisphere, then the magnitude of the momentum of the struck nucleon will be *less than* the magnitude of the three-momentum transfer,  $|\vec{p}_s| < |\vec{q}|$ . Compared to a nucleon of final momentum  $\vec{q}$ , the kinetic energy of the struck nucleon will be smaller and the energy transfer,  $\nu$ , will also be smaller so that  $x > 1$ . If the partner nucleon is detected in the backward hemisphere, then the magnitude of the momentum of the struck nucleon will be *greater than* the magnitude of the three-momentum transfer,  $|\vec{p}_s| > |\vec{q}|$ . In this case, the kinetic energy of the struck nucleon and hence the energy transfer will be greater so that  $x < 1$ .

Ref. [13] argues that the forward kinematics with smaller  $\nu$  and  $x > 1$  is preferred. They argue that these conditions, on the low-energy-transfer side of the  $(e, e')$  quasielastic peak, are farther from the region where meson exchange currents and  $\Delta$ -production can contribute. Therefore, cross sections measured at forward kinematics should be more sensitive to the short-range nucleon-nucleon correlations, *i.e.*, to the initial state momentum distribution.

On the contrary, Ref. [15] argues that the configuration where one proton is emitted backward is preferred. They argue that it is very difficult for Final State Interactions (FSI) to produce backward nucleons and therefore cross sections measured at backward kinematics will be more sensitive to the nuclear initial state. This argument is supported by  $d(e, e'p)$  measurements [16] where cross sections measured at backward proton angles agreed well with calculations that did not include FSI.

The present paper reports measurements of two proton knockout from  ${}^3\text{He}$  in both forward,  $x > 1$ , and backward,  $x < 1$ , kinematics in order to compare the measured relative momentum distributions and to determine which kinematic configuration is more sensitive to the initial state momentum distribution.

We measured the  ${}^3\text{He}(e, e'pp)n$  reaction at the Thomas Jefferson National Accelerator Facility (Jefferson Lab) in 2002 using a 100% duty factor, 5–10 nA beam of 4.7 GeV electrons incident on a 5-cm liquid  ${}^3\text{He}$  or  $\text{H}_2$  target. We detected the outgoing charged particles in the CEBAF Large Acceptance Spectrometer (CLAS) [17].

CLAS uses a toroidal magnetic field (with in-bending electrons) and six independent sets of drift chambers, time-of-flight scintillation counters and electro-magnetic calorimeters (EC) for charged particle identification and trajectory reconstruction. The polar angular acceptance is  $8^\circ < \theta < 140^\circ$  and the azimuthal angular acceptance is

50% at smaller polar angles, increasing to 80% at larger polar angles. The EC was used for the electron trigger with a threshold of approximately 0.9 GeV.

We eliminated the effects of interactions in the target walls by requiring particles to come from the central 4-cm of the target. We identified electrons using the energy deposited in the EC, and protons using time-of-flight. The  $\text{H}(e, e'p)$  cross section was measured and compared to a parametrization of the world's cross section data [18] to determine our electron and proton detection efficiencies [19].

Regions of non-uniform detector response were excluded by software cuts, while acceptance and tracking efficiencies were estimated using GSIM, the CLAS GEANT Monte-Carlo simulation [20]. Momentum coverage extended down to 0.35 GeV/c for protons.

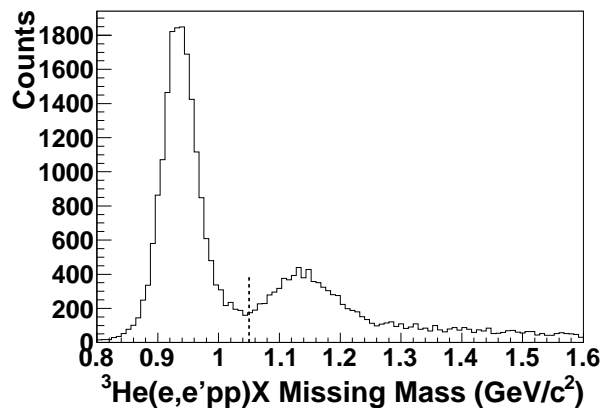


FIG. 1: Missing mass for  ${}^3\text{He}(e, e'pp)X$  for missing momentum  $p_X < 0.2$  GeV/c. The dashed vertical line indicates the neutron missing mass cut of  $M_X < 1.05$  GeV/c<sup>2</sup>.

We identified the neutron using a missing mass cut to select  ${}^3\text{He}(e, e'pp)n$  events (see Fig. 1). We required that each neutron had momentum  $p_n \leq 0.2$  GeV/c in order to focus on  $pp$  pairs with small total momentum. (Events with  $p_n \geq 0.25$  GeV/c are discussed in Ref. [10].) Fig. 2 shows that the experiment covered a wide range of energy and momentum transfers. For  ${}^3\text{He}(e, e'pp)n$  events, the momentum transfer  $Q^2$  peaks at around 1.5 GeV<sup>2</sup>. The energy transfer  $\nu$  is concentrated slightly above but close to quasielastic kinematics ( $\nu \approx Q^2/2m_p$  or  $x \approx 1$ ).

Since the two protons shared the energy and momentum transfer of the reaction, we looked at the opening angle of the two protons (see Fig. 3a). The distribution peaks at an opening angle of about  $80^\circ$ , characteristic of final state rescattering. (Nonrelativistically and classically, if one proton hits a second proton at rest, then the opening angle in the final state will be exactly  $90^\circ$ .) A one-body cross section calculation by Laget (described in detail below) integrated over the experimental acceptance does not show this rescattering peak, indicating

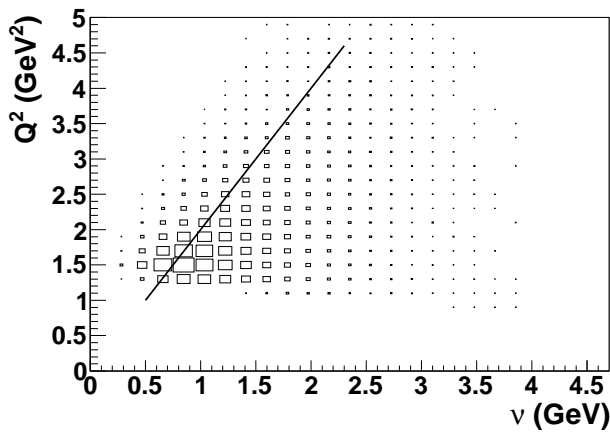


FIG. 2: The square of the four-momentum transfer,  $Q^2$ , versus the energy transfer  $\nu$  for  ${}^3\text{He}(e, e'pp)n$  events with  $p_n \leq 0.2$  GeV/c. The points show the data, the straight line shows quasielastic kinematics where  $x = Q^2/2m\nu = 1$ . The lower limit at  $Q^2 \approx 1$  GeV $^2$  is due to the CLAS acceptance.

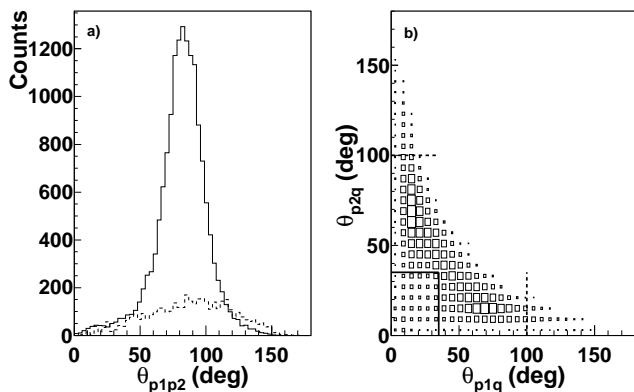


FIG. 3: a) The number of counts as a function of opening angle between the two protons in the lab frame for  ${}^3\text{He}(e, e'pp)n$  events for  $p_n < 0.2$  GeV/c for data (solid histogram) and the one-body calculation of Laget integrated over the experimental acceptance with arbitrary normalization (dashed histogram). b) The number of counts as a function of the two proton-momentum transfer angles,  $\theta_{p_1q}$  and  $\theta_{p_2q}$ .

that it is not an artifact of the experimental acceptance.

A two-dimensional plot of the opening angle between each proton and the momentum transfer,  $\vec{q}$ , (see Fig. 3b) shows peaks where one proton is at an angle of  $70^\circ$  with respect to  $\vec{q}$  and the other proton is at about  $15 - 20^\circ$ . These peaks are indicative of small angle rescattering, where one proton absorbs the virtual photon and scatters from the second proton in the final state. The first proton is slightly deflected from its original direction and the second proton is scattered at about  $70^\circ$ .

In order to study the contribution of different reaction mechanisms in different experimental configurations,

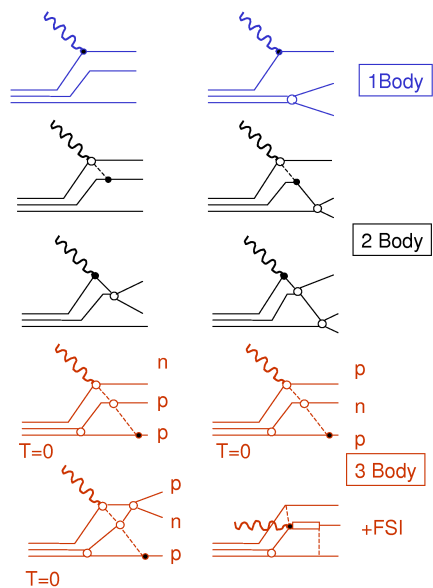


FIG. 4: (color online) The relevant graphs in the diagrammatic calculation of the  ${}^3\text{He}(e, e'pp)n$  reaction [21–24] including one-body, two-body, and three body mechanisms. The graph corresponding to Final State Interactions (as the term is used in this paper) is the middle graph on the left side.

we compared our data with the diagrammatic calculation of Laget. This calculates the differential cross section from the square of the coherent sum of the amplitudes associated with the diagrams in Fig. 4: the one-body, the two-body Final State Interactions or Meson Exchange Currents (MEC) and the three-body mechanisms. The antisymmetric bound state wave function is the solution [25] of the Faddeev equations for the Paris potential [26]. The continuum is approximated by the combination of the plane wave amplitudes and half off shell amplitudes where two nucleons scatter, the third being spectator. The antisymmetry of the final state is achieved by interchanging the role of the three nucleons. Two body MEC are computed as described in [23], while three body mechanisms are implemented as in [22].

Note that the one-body cross section is proportional to the initial state momentum distribution. This will be useful in helping us identify kinematic regions where the cross section is sensitive to the initial state.

The theoretical cross sections are then integrated by a Monte Carlo sampling of the phase space within the fiducial acceptance of CLAS and then binned in the same way as the experimental data.

At low energy, the application of the model to our channel, the electrodisintegration of a  $pp$  pair at rest, has been described in [21]. It has been adapted to higher energy according to [24]. The nucleon  $s$ -wave scattering has been supplemented by a high energy diffractive scattering amplitude that fits the experimental  $NN$  cross

section. It uses a fully relativistic nucleon current with the latest experimental values of the nucleon form factors. It describes well the two body [27] and three body [28] break up of  ${}^3\text{He}$  recently studied at Jefferson Lab in the same energy and momentum range.

The rescattering peak, near  $70^\circ$  in Fig. 3b, is more prominent than in the  ${}^2\text{H}(e, e'p)n$  reaction [29] under similar kinematics. The reason is that a  $pp$  pair at rest is almost entirely in a relative  $s$ -wave which has a node around  $400 \text{ MeV}/c$ : consequently the one-body contribution is strongly suppressed. Also, unlike in the  $pn$  channel [29], the contribution of the  $\Delta N$  intermediate state to the  $pp$  channel is very small. The reason is that a  $pp$  pair has no dipole moment for the virtual photon to couple to. If a virtual photon is absorbed on a  $pp$  pair at rest, it would create a  $\Delta N$  system in a  $1^+$  state which cannot then decay into a  $pp$  system (see e.g., Ref. [21]).

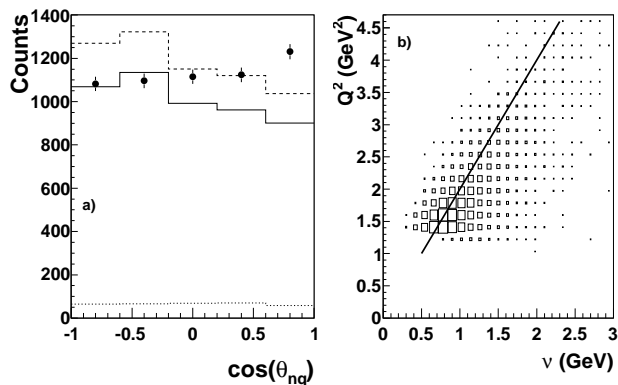


FIG. 5:  ${}^3\text{He}(e, e'pp)n$  events with  $p_n < 0.2 \text{ GeV}/c$  and  $0.4 \leq p_p^{\text{slow}} \leq 0.6 \text{ GeV}/c$  (where  $p_p^{\text{slow}}$  is the smaller of the two proton momenta): a) The number of counts plotted versus  $\cos\theta_{nq}$ , the angle between the neutron momentum and  $\vec{q}$ . The points show the data, the dotted curve shows Laget's one-body calculation, the dashed curve includes final state interactions, and the solid curve shows the full calculation including FSI and meson exchange currents [21–24]. For ease of comparison of the angular distributions, the theoretical calculations are all multiplied by the same arbitrary factor to approximately scale the full calculation to the data. The data and the calculations are all approximately isotropic. b) The number of counts plotted as a function of the four-momentum transfer squared and the energy transfer ( $Q^2$  and  $\nu$ ). The points show the data, the straight line shows quasielastic kinematics where  $x = Q^2/2m\nu = 1$ .

In order to test the hypothesis that most of the  ${}^3\text{He}(e, e'pp)n$  events are dominated by final state rescattering and to validate the calculation, we looked at the distribution of events with  $0.4$  to  $0.6 \text{ GeV}/c$  protons. These protons will always be the slower of the two protons in the reaction. This momentum range was selected to maximize the expected effects of final state interactions.

If these events are dominated by proton knockout followed by  $pp$  rescattering, then the neutron should be spectator to the reaction and its angular distribution with respect to the momentum transfer  $\vec{q}$  should be isotropic (see Fig. 5a). This agrees with the calculation both without and with FSI. The inclusion of FSI increases the magnitude of the calculation by more than an order of magnitude and the inclusion of Meson Exchange Currents (MEC) changes it by only another 20%.

The momentum and energy transfer distribution for these events is shown in Fig. 5b. The energy and momentum transfers are centered around  $x = 1$ , as expected for quasielastic knockout with or without subsequent rescattering.

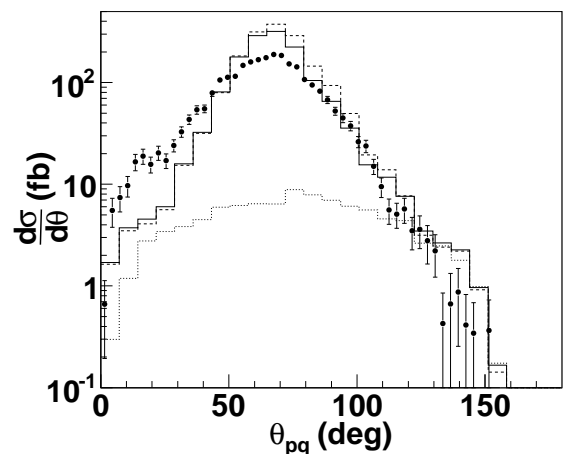


FIG. 6: The laboratory-frame cross section for  ${}^3\text{He}(e, e'pp)n$  events with  $p_n < 0.2 \text{ GeV}/c$  and  $0.4 \leq p_p^{\text{slow}} \leq 0.6$  plotted versus  $\theta_{pq}$ , the opening angle between the proton momentum,  $\vec{p}_p^{\text{slow}}$ , and the momentum transfer  $\vec{q}$ . The points show the data, the dotted curve shows Laget's one-body calculation, the dashed curve includes final state interactions, and the solid curve shows the full calculation including FSI and meson exchange currents [21–24]. No scale factors have been applied to the calculations. Systematic uncertainties of 15% are not shown.

Fig. 6 shows the cross section as a function of the angle between the slower proton ( $0.4 \leq p_p^{\text{slow}} \leq 0.6 \text{ GeV}/c$ ) and  $\vec{q}$ . The cross sections are corrected for radiative effects and tracking efficiency and then integrated over the experimental acceptance [19]. The systematic uncertainty is 15%, primarily due to the uncertainty in the low momentum proton detection efficiency. The data distribution has a prominent peak at around  $70^\circ$ . The calculation including the effects of FSI agrees qualitatively with the data, peaking at around  $\theta_{pq} \approx 70^\circ$  at a cross section more than ten times larger than that of the one-body calculation. This shows that the prominent peaks seen at  $\theta_{pq} \approx 70^\circ$  in Fig. 3b are due to FSI. Note that the

model only takes into account the dominant diffractive scalar part of the  $pp$  scattering amplitude, and the inclusion of the full experimental amplitude (from the SAID data base for instance) may likely improve the agreement between data and model.

The comparison between data and calculation for  $0.4 \leq p_p^{slow} \leq 0.6$  GeV/c shows that the cross section is dominated by FSI and that the calculation qualitatively agrees with the data.

The next step in the analysis was to try to identify kinematic configurations that are sensitive to high-momentum components of the momentum distribution and which are not significantly affected by FSI. (MEC are suppressed for  $pp$  knockout because the virtual photon does not couple strongly to neutral pions.) To do that we looked at events where one proton is emitted backward with respect to the momentum transfer,  $\theta_{pq} \geq 100^\circ$ , as shown by the dashed lines in Fig. 3b. Because it is difficult for FSI to produce backward-going nucleons, many theorists expect that this kinematics will be the most sensitive to the nuclear initial state [15].

We also looked at events where both protons are emitted forward. This kinematics was chosen because it corresponds to  $x > 1$ , on the low energy-loss side of the quasielastic peak, where there are smaller contributions to the  $(e, e')$  cross section from meson exchange currents and delta isobar currents. Several short range correlations experiments [13, 30] have chosen to measure cross sections at  $x > 1$ . However, when both protons are emitted forward they have smaller relative momentum in the final state and hence will have larger final state interactions. This increased FSI will complicate the interpretation of the data.

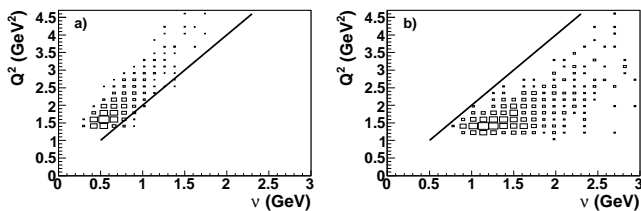


FIG. 7: The square of the four-momentum transfer,  $Q^2$ , versus the energy transfer  $\nu$  for  ${}^3\text{He}(e, e'pp)n$  events with  $p_n \leq 0.2$  GeV/c; a) with two forward protons. Both protons are within  $35^\circ$  of the momentum transfer,  $\theta_{p_1q}$  and  $\theta_{p_2q} \leq 35^\circ$ ; and b) with one forward and one backward proton such that  $\theta_{pq} \geq 100^\circ$ . The points show the data, the straight line shows quasielastic kinematics where  $x = Q^2/2m\nu = 1$ .

Fig. 7 shows the momentum- and energy-transfer distributions for the two-forward-proton (“forward”) and the backward-proton (“backward”) kinematics. As expected, the forward kinematics is at lower energy loss and  $x > 1$  and the backward kinematics is at higher energy loss and  $x < 1$ . The neutron angular distributions for the two kinematics are shown in Fig. 8. These neu-

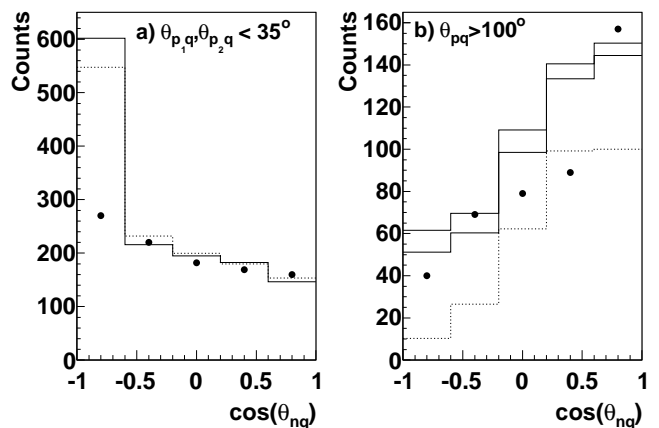


FIG. 8: The angular distribution of  $p_n \leq 0.2$  GeV/c neutrons with respect to the momentum transfer  $\vec{q}$ , for  ${}^3\text{He}(e, e'pp)n$  events a) with two forward protons,  $\theta_{p_1q}, \theta_{p_2q} \leq 35^\circ$ , and b) with one backward proton  $\theta_{pq} \geq 100^\circ$ . The points show the data, the histograms are the same as in Fig. 6. For ease of comparison of the angular distributions, the calculations have been separately normalized for the two plots so that the full calculation (solid line) is approximately equal to the data.

tron distributions are not as isotropic as for the events with moderate momentum protons (see Fig. 5b). This is due to the initial state momentum distribution, since it is also seen in the angular distribution of Laget’s one-body calculation.

For both forward and backward kinematics we calculated the “ $q$ -subtracted” relative momentum,

$$p_{rel} = \frac{1}{2} |\vec{p}_1 - \vec{q} - \vec{p}_2| \quad .$$

For the forward kinematics, we chose proton 1 such that  $p_1 > p_2$ . For the backward kinematics we chose proton 1 to be the forward proton. In the one-body limit (*i.e.*, in the absence of FSI, MEC and IC), the “ $q$ -subtracted” relative momentum equals the relative momentum of the two protons in the initial state.

The measured relative momentum distributions for the forward and backward kinematics (see Fig. 9) are very different. The forward proton  $p_{rel}$  distribution peaks at significantly higher momentum and is much broader than the backward proton distribution. This strongly indicates that at least one of the two distributions is not sensitive to the initial state momentum distribution. The minimum detected proton momentum of  $p_p > 0.35$  GeV/c restricts the minimum measurable relative momentum.

Calculations by Laget indicate that the forward proton kinematics is much more sensitive to FSI. FSI only affects the backward kinematics at  $p_{rel} \approx 0.4$  GeV/c by filling in the minimum of the  $pp$  momentum distribution. However, FSI increases the cross section by a factor of at least three in forward kinematics for all relative momenta

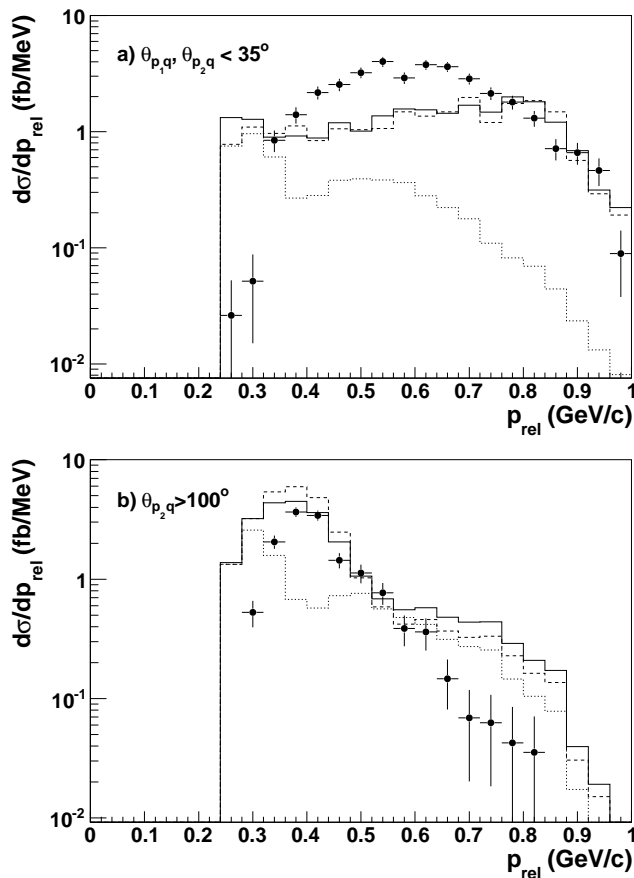


FIG. 9: The  ${}^3\text{He}(e, e'pp)n$  laboratory-frame cross section plotted versus the “ $q$ -subtracted” relative momentum,  $p_{rel} = |\vec{p}_1 - \vec{q} - \vec{p}_2|/2$ , for events with a) both protons forward,  $\theta_{p_1q}, \theta_{p_2q} \leq 35^\circ$  and b) one proton backward,  $\theta_{p_2q} \geq 100^\circ$ . The points show the data, the dotted line shows the one-body calculation, the dashed line shows the one-body + FSI calculation, and the solid line shows the full calculation including FSI and MEC. No scale factors have been applied to the calculations.

greater than 0.4 GeV/c. This is not surprising, since the final state relative momentum,  $p_{rel}^f = |\vec{p}_1 - \vec{p}_2|/2$ , is significantly smaller for the forward kinematics, leading to a larger final state interaction.

The Laget calculation agrees qualitatively with the data for  $p_{rel} > 0.4$  GeV/c in both kinematics. In the forward kinematics the full cross section is several times larger than the one-body cross section at  $p_{rel} > 0.4$  GeV/c, indicating that the cross section is dominated by the effects of FSI (see Fig. 9a). Note that  $pp$  rescattering in the final state (FSI) redistributes strength from lower to higher relative momenta. Thus, the calculated cross section at large relative momenta depends on the initial state momentum distribution at much smaller momenta and on the details of the  $pp$  rescattering model.

The full calculation underestimates the forward proton cross section for  $0.4 < p_{rel} < 0.7$  GeV/c. Because the

cross section in this region is dominated by FSI, this underestimate indicates the need to include the full rescattering amplitude (including spin-dependent parts) and not just its dominant diffractive (scalar) part.

In the backward kinematics (Fig. 9b) Laget’s calculation overestimates the backward proton cross sections for  $p_{rel} > 0.6$  GeV/c. The full calculation is very close to the one-body calculation in this region, indicating that FSI effects are small and that the cross section is dominated by the initial state momentum distribution. Thus this overestimate indicates that the wave function used (a Faddeev solution of the Paris potential) contains too much high-momentum strength. Disagreement at these large momenta is not surprising, because  $NN$  potential models (and hence calculated initial state momentum distributions) are poorly constrained by elastic scattering data for  $p_{rel} > 0.35$  GeV/c, where inelastic channels open up.

Using a different nuclear wave function with a different initial state momentum distribution could increase agreement between data and calculation at the backward kinematics without decreasing agreement at the forward kinematics. The forward kinematics cross section is dominated by FSI, that is by  $pp$  rescattering which redistributes strength from lower to higher relative momenta. Therefore decreasing the strength of the initial state momentum distribution at  $p_{rel} > 0.6$  GeV/c would not significantly change the calculated cross sections at forward kinematics and therefore would not affect the agreement between data and calculation for the forward kinematics at  $p_{rel} > 0.6$  GeV/c.

In summary, the large kinematics coverage of CLAS allowed us to identify the important reaction ingredients in various portions of the phase space when the neutron is almost a spectator. The data confirm the expectations of a model which combines the dominant parts of the amplitudes: the Faddeev three body wave function, final state interactions using the dominant diffractive scalar part of the  $NN$  scattering amplitude, and the MEC and  $\Delta$  formation amplitudes. Proton-proton rescattering dominates the cross section around  $x = 1$ . MEC and  $\Delta$  formation contributions are relatively small.

We compared the  $q$ -subtracted relative momentum distributions for kinematics with a low-momentum (spectator) neutron in two configurations: (1) with both protons emitted in the forward direction and (2) with one proton emitted forward and the other backward. The full calculation and the data agree qualitatively at both kinematic configurations. The calculation shows that for  $p_{rel} > 0.5$  GeV/c, FSI are very small at the backward kinematics but are dominant at the forward kinematics. Thus, the cross section measured at backward kinematics is much closer than that measured at forward kinematics to the one-body calculation, and hence is much more sensitive to the initial state momentum distribution.

This result indicates that short range correlations stud-

ies using two-nucleon knockout experiments to measure the  $NN$  relative momentum distribution should concentrate on kinematics at  $x < 1$  where one of the nucleons is emitted backward.

We acknowledge the outstanding efforts of the staff of the Accelerator and Physics Divisions (especially the CLAS target group) at Jefferson Lab that made this experiment possible. This work was supported in part by the Italian Istituto Nazionale di Fisica Nucleare, the Chilean CONICYT, the French Centre National de la Recherche Scientifique and Commissariat à l’Energie Atomique, the UK Science and Technology Facilities Council (STFC), the U.S. Department of Energy and National Science Foundation, and the National Research Foundation of Korea. Jefferson Science Associates, LLC, operates the Thomas Jefferson National Accelerator Facility for the United States Department of Energy under contract DE-AC05-06OR23177.

---

\* Current address: University of Virginia, Charlottesville, Virginia 22901

† Contact Author weinstein@odu.edu

‡ Current address:CEA, Centre de Saclay, Irfu/Service de Physique Nucléaire, 91191 Gif-sur-Yvette, France

§ Current address:Skobeltsyn Nuclear Physics Institute, Skobeltsyn Nuclear Physics Institute, 119899 Moscow, Russia

¶ Current address:INFN, Sezione di Genova, 16146 Genova, Italy

\*\* Current address:Argonne National Laboratory, Argonne, Illinois 60439

- [1] J. Kelly, Adv. Nucl. Phys. **23**, 75 (1996).  
 [2] K. Egiyan et al. (CLAS Collaboration), Phys. Rev. C **68**, 014313 (2003).  
 [3] K. Egiyan et al. (CLAS Collaboration), Phys. Rev. Lett. **96**, 082501 (2006).  
 [4] N. Fomin et al., Phys. Rev. Lett. **in press** (2012).  
 [5] L. Frankfurt and M. Strikman (AIP, 2008), eds. S. Boffi, et al., vol. 1056, pp. 241–247.  
 [6] L. B. Weinstein, E. Piasezky, D. W. Higinbotham, J. Gomez, O. Hen, and R. Shneor, Phys. Rev. Lett. **106**, 052301 (2011).  
 [7] S. A. Kulagin and R. Petti, Phys. Rev. C **82**, 054614 (2010).  
 [8] L. Frankfurt, M. Strikman, D. Day, and M. Sargsyan, Phys. Rev. C **48**, 2451 (1993).  
 [9] R. Niyazov et al. (CLAS Collaboration), Phys. Rev. Lett. **92**, 052303 (2004).  
 [10] H. Baghdasaryan et al. (CLAS Collaboration), Phys. Rev. Lett. **105**, 222501 (2010).  
 [11] A. Tang et al., Phys. Rev. Lett. **90**, 042301 (2003).  
 [12] E. Piasezky, M. Sargsian, L. Frankfurt, M. Strikman, and J. W. Watson, Phys. Rev. Lett. **97**, 162504 (2006).  
 [13] R. Shneor et al., Phys. Rev. Lett. **99**, 072501 (2007).  
 [14] R. Subedi et al., Science **320**, 1476 (2008).  
 [15] W. Melnitchouk, M. Sargsian, and M. Strikman, Z. Phys. A **359**, 99 (1997).  
 [16] A. V. Klimenko et al. (CLAS Collaboration), Phys. Rev. C **73**, 035212 (2006).  
 [17] B.A. Mecking et al., Nucl. Inst. and Meth. **A503**, 513 (2003).  
 [18] J. Arrington, Phys. Rev. C **68**, 034325 (2003).  
 [19] H. Baghdasaryan, Ph.D. thesis, Old Dominion University, Norfolk, VA (2007).  
 [20] CLAS GEANT Simulation, Tech. Rep. (1997), URL <http://nuclear.unh.edu/~maurik/Gsim/>.  
 [21] J.-M. Laget, Phys. Rev. C **35**, 832 (1987).  
 [22] J.-M. Laget, J. Phys. G **14**, 1445 (1988).  
 [23] J.-M. Laget, Nucl. Phys. **A579**, 333 (1994).  
 [24] J.-M. Laget, Phys. Lett. **B609**, 49 (2005).  
 [25] C. Hajduk and P. U. Sauer, Nucl. Phys. **A322**, 329 (1979).  
 [26] M. Lacombe et al., Phys. Lett. B **101**, 139 (1981).  
 [27] M. M. Rvachev et al. (Jefferson Lab Hall A Collaboration), Phys. Rev. Lett. **94**, 192302 (2005).  
 [28] F. Benmokhtar et al. (Jefferson Lab Hall A Collaboration), Phys. Rev. Lett. **94**, 082305 (2005).  
 [29] K. S. Egiyan et al. (CLAS Collaboration), Phys. Rev. Lett. **98**, 262502 (2007).  
 [30] E. Piasezky et al., *Jefferson Lab Expt E07-006, Studying Short-Range Correlations in Nuclei at the Repulsive Core Limit via the Triple Coincidence ( $e, e'pN$ ) Reaction* (2007), URL <http://hallaweb.jlab.org/experiment/E07-006/>.